## Appendix A: Empirical equations used to compute properties of water

The properties of water of interest within this project include the compressional wave velocity, density, bulk modulus and viscosity. These were calculated from the temperature and salinity of the water using standard empirical relationships obtained from the literature and assuming a pressure of 1 atmosphere. Velocity was calculated using merged equations (Lovett, 1978) and is required to predict the pressure field emitted by the SPADE source during calibration water tests and compare predicted values to those measured, *Section 4.3*. Density, bulk modulus and viscosity are obtained from standard equations of state (Siedler, 1986) and are required as input parameters for Biot Theory, *Section 7.1.1.* The details of the empirical relationships are included below.

- The compressional wave velocity $v_w$ was computed using

$$v_w = v_1 + v_T + v_S + v_P + v_{TSP} \qquad A.1a,$$

where

$$v_1 = 1402.394 \qquad A.1b,$$

$$v_T = 5.01132 \cdot T - 5.513036 \cdot 10^{-2} \cdot T^2 + 2.221008 \cdot 10^{-4} \cdot T^3 \qquad A.1c,$$

$$v_S = 1.332947 \cdot S \qquad A.1d,$$

$$v_P = 1.605336 \cdot 10^{-2} \cdot P + 2.12448 \cdot 10^{-7} \cdot P^2 \qquad A.1e,$$

$$\begin{aligned} v_{TSP} = {} & -1.266383 \cdot 10^{-2} \cdot T \cdot S + 9.543664 \cdot 10^{-5} \cdot T^2 \cdot S \\ & - 1.052396 \cdot 10^{-8} \cdot T \cdot P^2 + 2.183988 \cdot 10^{-13} \cdot T \cdot P^3 \\ & - 2.253828 \cdot 10^{-13} \cdot S \cdot P^3 + 2.062107 \cdot 10^{-8} \cdot T \cdot S^2 \cdot P \end{aligned} \qquad A.1f.$$

As the ranges of temperature and salinity for which *Equations A.1* are valid are not quoted in the relevant literature, these are assumed to be the ranges spanned by the velocity data used to derive the empirical relationships, *i.e.* temperatures from –3 to 40 $^{o}$C and salinities from 0 to 41 ‰ (Wilson *et al* 1960, Del Grosso *et al* 1972).

- The density $\rho_f$ was computed for a pressure of one atmosphere from the international equation of state of seawater,

$$\rho_f(S,T) = \rho_w(T) + F_1(T) \cdot S + F_2(T) \cdot S^{3/2} + 4.8314 \cdot 10^{-4} \cdot S^2 \qquad A.2a,$$

where

$$F_1(T) = 0.8245 - 4.0899 \cdot 10^{-3} \cdot T + 7.6438 \cdot 10^{-5} \cdot T^2 - 8.2467 \cdot 10^{-7} \cdot T^3 + 5.3875 \cdot 10^{-9} \cdot T^4 \quad \textit{A.2b,}$$

$$F_2(T) = -5.7247 \cdot 10^{-3} + 1.0227 \cdot 10^{-4} \cdot T - 1.6546 \cdot 10^{-6} \cdot T^2 \quad \textit{A.2c,}$$

and the density of pure water $\rho_w(T)$ is obtained from

$$\rho_w(T) = 999.4226 + 6.794 \cdot 10^{-2} \cdot T - 9.0953 \cdot 10^{-3} \cdot T^2 + 1.0017 \cdot 10^{-4} \cdot T^3 - 1.1201 \cdot 10^{-6} \cdot T^4 + 6.5363 \cdot 10^{-9} \cdot T^5 \quad \textit{A.2d.}$$

*Equations A.2a* to *A.2d* are valid for salinities between 0 and 42 ‰ and temperatures from – 2 to 40 $^{o}$C.

- The bulk modulus of the pore water $K_f$ at a pressure of one atmosphere was computed using

$$K_f(S,T) = K_w + F_3(T) \cdot S + F_4(T) \cdot S^{3/2} \quad \textit{A.3a,}$$

where

$$F_3(T) = 546.746 - 6.0346 \cdot T + 1.0999 \cdot 10^{-1} \cdot T^2 - 6.167 \cdot 10^{-4} \cdot T^3 \quad \textit{A.3b,}$$

$$F_4(T) = 0.7944 + 0.1648 \cdot T - 5.3009 \cdot 10^{-3} \cdot T^2 \quad \textit{A.3c,}$$

and the bulk modulus of pure water $K_w(T)$ is obtained from

$$K_w(T) = 1.9652 \cdot 10^5 + 1484.206 \cdot T - 23.271 \cdot T^2 + 0.137 \cdot T^3 - 5.155 \cdot 10^{-4} \cdot T^4 \quad \textit{A.3d.}$$

*Equations A.3a* to *A.3d* are again valid for salinities between 0 and 42 ‰ and temperatures from – 2 to 40 $^{o}$C.

- The viscosity of the pore water $\eta$ at one atmosphere was calculated from

$$\eta(S,T) = \eta_1(T) + F_5(T) \cdot Cl^{1/2} + F_6(T) \cdot Cl \quad \textit{A.4a,}$$

where

$$F_5(T) = 1.0675 \cdot 10^{-4} + 5.185 \cdot 10^{-5} \cdot T \quad \textit{A.4b,}$$

$$F_6(T) = 2{,}591 \cdot 10^{-3} + 3.3 \cdot 10^{-5} \cdot T \quad \textit{A.4c,}$$

and $\eta_1(T)$ is the viscosity of pure water as a function of temperature which is obtained from

$$\eta_1(T) = 1.002 \cdot 10^{-3} \cdot 10^{F_7(T)} \quad \textit{A.4d,}$$

with

$$F_7(T) = \frac{1.1709 \cdot (20 - T) - 1.827 \cdot 10^{-3} \cdot (T - 20)^2}{T + 89.93} \qquad A.4e.$$

The variable *Cl* denotes volume chlorinity, which is related to salinity through

$$Cl = \frac{\rho_w S}{1806.55} \qquad A.5.$$

Equations A.4a *to* A.4e are valid for salinities from 0 to 40 ‰ and temperatures from 10 to 70 $^{o}$C.

## Appendix B: Additional details of fieldsites examined

Additional details of the fieldsites, which are not included in *Section 4.4.2,* are displayed in *Table B.1.* These include the date on which each location was examined, position of the source, orientation of the central receiver line to the source and depths at which the probes were deployed. Relevant location specific details are listed below:

- At the Studland site large pebbles and shells with diameters up to 15 cm were observed at locations 1 and 4. No information was available concerning the orientation of the receiver line at Locations 1 and 2, and concerning the position of the source at Location 1. The depth of the probes ranged from 0.8 to 0.95 m at Location 2 due to wave scouring.
- At the Lilliput site organic root material was observed in the sediment to a depth of 0.3 m at Location 1 and 0.7 m at Location 4.
- At the silts sites rubble was observed on the surface of the sediment at a number of locations.
- At the Needs Ore site a pebble layer was observed at sediment depths of 0.1 to 0.2 m at Locations 1 and 3, while a more consolidated layer of sediment existed from depths of 1 m at Locations 1 and 2. The reduced depth of the probes at these locations, *i.e.* 0.7 and 0.8 m, minimises interference of signals reflected from this sediment horizon.
- A reed bed lay within 1 m of Mercury 1 and gas bubbles were observed on the insertion of the probes. In addition scattering centres were identified at Mercury 1, 2 and 3, in the form of wood sections which lay up to 0.3 m deep.
- At the Saltern site a peaty layer was observed to lie 0.8 to 0.9 m below the surface and hence the probe depth was reduced to 0.65 to 0.7 m. Plastic pipes with lengths of 0.5 m and diameters of 0.1m were observed within the sediment to a depth of 0.3 m at Location 2.
- Grain size analysis yielded limited information concerning the materials present within the sediment. These included; organic material in the sand fractions of Needs Ore 1 and 2 and Saltern 1; slate fragments in the $<0\ \phi$ portion at Branksome 3 and shells with diameters less than 2 mm within the sand portion at Needs Ore 3.

| General Fieldsite | Location examined | Date tested | Position of source | Orientation of receivers | Probe depth (m) |
|---|---|---|---|---|---|
| Studland | 1 | 26-07-02 | - | - | 1.0 |
| | 2 | 13-09-02 | N 50° 40’ 714’’ W 001° 56’ 971’’ | - | 1.0 |
| | 3 | 18-09-02 | N 50° 40’ 710’’ W 001° 56’ 939’’ | 125° | 0.8 - 0.95 |
| | 4 | 27-09-02 | N 50° 40’ 701’’ W 001° 56’ 927’’ | 320° | 1.0 |
| Branksome | 1 | 11-10-02 | N 50° 42’ 403’’ W 001° 54’ 491’’ | 230° | 0.9 |
| | 2 | 16-10-02 | N 50° 42’ 392’’ W 001° 54’ 491’’ | 235° | 1.0 |
| Lilliput | 1 | 25-09-02 | N 50° 40’ 714’’ W 001° 55’ 908’’ | 180° | 1.0 |
| | 2 | 02-10-02 | N 50° 41’ 698’’ W 001° 55’ 908’’ | 195° | 1.0 |
| | 3 | 25-10-02 | N 50° 41’ 696’’ W 001° 55’ 906’’ | 180° | 1.0 |
| | 4 | 29-10-02 | N 50° 41’ 722’’ W 001° 55’ 912’’ | 160° | 1.0 |
| Needs Ore Point | 1 | 08-11-02 | N 50° 46’ 650’’ W 001° 23’ 710’’ | 290° | 0.7 |
| | 2 | 15-11-02 | N 50° 46’ 648’’ W 001° 23’ 749’’ | 290° | 0.8 |
| | 3 | 28-10-02 | N 50° 46’ 648’’ W 001° 23’ 713’’ | 280° | 1.0 |
| Mercury | 1 | 12-11-02 | N 50° 52’ 598’’ W 001° 18’ 808’’ | 70° | 1.0 |
| | 2 | 13-11-02 | N 50° 52’ 388’’ W 001° 18’ 818’’ | 40° | 1.0 |
| | 3 | 12-12-02 | N 50° 52’ 380’’ W 001° 18’ 823’’ | 240° | 1.0 |
| Saltern | 1 | 26-11-02 | N 50° 52’ 586’’ W 001° 18’ 739’’ | 100° | 0.65 – 0.7 |
| | 2 | 27-11-02 | N 50° 52’ 572’’ W 001° 18’ 709’’ | 280° | 0.95 – 1.0 |
| Universe | 1 | 01-11-02 | N 50° 52’ 536’’ W 001° 18’ 164’’ | 0° | 1.0 |
| | 2 | 11-11-02 | N 50° 52’ 547’’ W 001° 18’ 175’’ | 0° | 1.0 – 1.15 |

*Table B.1. Additional details of fieldsites examined, including date on which each location was examined, position of source, orientation of central receiver line to source and depths at which probes were deployed.*

# Appendix C: Measurement of geotechnical properties of sediments

The geotechnical properties of the sediment which are measured include porosity, bulk density, mean grain diameter and percentage of sand sized particles. These have been defined in *Section 2.1*, with the resulting values presented in *Section 4.4.3*. This Appendix will describe the standard techniques used to measure these properties. Prior to testing the sediment samples collected during the fieldwork were stored at temperatures less than 0 $^{o}$C in order to prevent bacterial action from altering the samples (Christian and Karl, 1995).

## C.1. Measurement of porosity and bulk density

For each location, one sediment sample was processed to obtain porosity. This involved depositing the sample in a measuring cylinder containing water and allowing the sample to settle for 24 to 72 hours, which ensured the settled sediment was fully saturated. The water column above the sediment was then siphoned off and the saturated mass and saturated volume of the sediment measured. The sediment was transferred to a metal container and dried at 100 $^{o}$C for a period of 24 to 48 hours. The dry mass was then measured and percentage porosity $n$ calculated from

$$n = 100 \cdot \frac{\left(M_T - M_D\right) \Big/ \rho_w}{V_S} \qquad \text{C.1,}$$

where $M_T$ is the saturated mass in kg, $M_D$ the dry mass in kg, $\rho_w$ the density of pure water (1000 kg·m$^{-3}$ at standard temperature and pressure) and $V_S$ the saturated volume, in m$^3$.

It was necessary to correct for the weight of dried salts present in the dried sediment, which will produce a porosity that is lower than the true value. This was achieved empirically by multiplying the measured porosity by a factor of 1.012 (Hamilton, 1971b). As the salinities of the inter-tidal sites examined within this project are less than those of the marine sediments for which this empirical correction factor is obtained (see *Section 4.4.3*) the above correction may result in over-estimates of porosity, with a maximum possible over-estimate of 1.2 %.

The bulk density $\rho$ was calculated from *Equation C.2* with no corrections required (Hamilton, 1971b).

$$\rho = \frac{M_T}{V_W} \qquad C.2,$$

Though the basic technique used was the same for coarse-grained and fine-grained sediments, the samples analysed in each case differed. Firstly, the typical weights of the samples analysed differed, with coarse-grained sediment samples weighing approximately 1 kg and fine-grained samples weighing approximately 100 g. Secondly, for the case of fine-grained sediments, the original samples could not be directly used, as these resulted in porosities more typically associated with sands. This was a consequence of the sample remaining in its original shape and drying in a block, which retained water in its centre. On dissection the texture of the block was observed to differ between the centre and the edges. Hence it was necessary to pass the fine-grained sediments through a 63μm sieve before allowing them to settle. This allowed all water to be removed during the drying stage.

The intrinsic disadvantages of the technique used to measured porosity and density are that the structure of the sediment is broken up and the settling times utilised in the laboratory are much less than those present *in situ*. Hence measured porosities and densities may not be representative of *in situ* values, the implications of which are discussed in *Section 4.4.3*.

The errors in the porosity and bulk density were calculated by propagating the measurement errors through the *Equations C.1* and *C.2*. These measurement errors include an accuracy of $\pm$ $1 \cdot 10^{-5}$ kg in saturated and dry masses, $\pm$ $5 \cdot 10^{-6}$ $m^3$ in saturated volume and $\pm$ 2 $kg \cdot m^{-3}$ in the density of water. The error in the density of water was obtained from the deviation of the pore water density from its mean value of 1001 $kg \cdot m^{-3}$, *Table 7.1* in *Section 7.1*. The resulting errors in porosity $n_e$ and bulk density $\rho_e$ were therefore obtained from

$$n_e = n \cdot \sqrt{\left(\frac{2 \cdot 10^{-5}}{M_T - M_D}\right)^2 + \left(\frac{2}{1001}\right)^2 + \left(\frac{5 \cdot 10^{-6}}{V_W}\right)^2} \qquad C.3,$$

$$\rho_e = \rho \cdot \sqrt{\left(\frac{1 \cdot 10^{-5}}{M_T}\right)^2 + \left(\frac{5 \cdot 10^{-6}}{V_W}\right)^2} \qquad C.4.$$

As the typical weight of silt samples analysed was much less than that of the sand samples, errors in measured porosity and bulk density are greater for silts than for sands (see *Section 4.4.3*).

### A3.2. Measurement of grain size parameters

For each location three or more samples were selected to span the region from the position of the source to that of the furthest receiver. Pre-analysis sample preparation typically includes:

- the removal of organic material using ashing or chemical processes.
- the removal of carbonates, e.g. shells, using chemical processes.
- the removal of iron oxides, again using chemical processes.
- the removal of salts, through rinsing of the sample with distilled water.

This project is interested in any material present in the sediment which can affect the propagation of acoustic waves. This includes organic and carbonate material, which can act as a scattering centre and affect the structure of the sediment and the number and nature of inter-grain contacts. Layers of iron oxides form on the surface of sediment grains (Mebra and Jackson, 1960) and will affect both the size of the grains and the cementation of the inter-grain contacts. Hence these substances should not be removed from the samples. The removal of salts is however advantageous. Though this was achieved for the sand fraction during the wet sieving stage, time limitations prevented this being undertaken for the mud fraction. This may bias the percentage of sand sized particles obtained to lower values, while the use of defloccuant should prevent the presence of salts from affecting the grain size distributions obtained for the mud fraction.

The preliminary stage of the grain size analysis was to reduce the size of the samples collected in order to obtain a usable and consistent sample size. This was achieved using a "cone approach", which involved depositing the original sample on a clean surface in a cone. The required mass of sediment, approximately 200 g for sands and 50 g for silts, was obtained by selecting opposing segments of this cone. This procedure obtains an unbiased sub-sample from an original sample that may be biased owing to the settling of heavier, coarser particles during collection and transportation.

This sub-sample was then wet sieved through a 63 μm sieve in order to separate the sand and mud fractions, which are defined as particles with diameters greater than 63 μm and less than 63 μm respectively (McManus, 1989). This is necessary to allow subsequent analysis of the two fractions. The sand fraction was then dried in an oven, for at least 48 hours at 100 $^{o}$C, after which the dry mass was recorded. This drying process requires the preliminary removal of muds, the presence of which will cement the sand

particles together. The mud fraction was allowed to settle for at least 48 hours, excess water siphoned off and concentrated mud sample stored. The two fractions were then analysed separately.

The sand fraction was analysed using a ¼ $\phi$ sieve stack, with a range of mesh sizes from 0 $\phi$ (1 mm) to 4 $\phi$ (63 μm). A recommended weight of approximately 100 g (McManus, 1989) of the dried sand fraction was selected and weighed. This was then passed though the sieve sizes listed in *Table C.1*, using a mechanical shaker, the vibrations of which were maintained at a constant amplitude and duration for all samples. The mass retained by each sieve was noted. The sum of these masses allowed a sieving error, *i.e*. the percentage of sample lost in sieving process, to be determined. For all but two samples this was less than 1.33 %, which is acceptable (Davies, 2003). The remaining two samples had errors of 2.65 % and 7.51 %, results from which will be considered with caution.

| Aperture (mm) | Aperture (ϕ) |
|---|---|
| 1.000 | 0.00 |
| 0.840 | 0.25 |
| 0.710 | 0.5 |
| 0.590 | 0.75 |
| 0.500 | 1.00 |
| 0.420 | 1.25 |
| 0.350 | 1.50 |
| 0.300 | 1.75 |
| 0.250 | 2.00 |
| 0.210 | 2.25 |
| 0.177 | 2.50 |
| 0.149 | 2.75 |
| 0.125 | 3.00 |
| 0.105 | 3.25 |
| 0.088 | 3.50 |
| 0.074 | 3.75 |
| 0.063 | 4.00 |

*Table C.1. Aperture of sieves used in grain size analysis, in units of mm* and *$\phi$.*

The mud fraction was analysed using a Coulter LS130 particle size analyser, which can measure grain sizes from 0.1 μm to 900 μm (Coulter, 1994). This measures the scatter

of laser light, with a wavelength of 750 nm, from a suspension of particles in an optical cell. The percentage volume of the sample (Coulter, 1994) contained in a suite of grain size ranges is determined using a Fraunhoffer scattering model. In order to prevent bias, the concentrate mud fraction was well mixed with water before a pipette sample is taken. This was diluted and ten drops of 0.5 % Sodium Hexametaphosphate solution added to prevent the flocculation of particles. This is the maximum recommended amount of deflocculant agent that can be added, with larger amounts resulting in the generation of bubbles in the optical cell, which will disrupt the diffraction of the laser light(Coulter, 1994). The deflocculant works by the absorption of highly charged anions onto the sediment particles, thus creating strong repulsive forces between particles which were previously attracted to each other. A fraction of this diluted sample is then added to the optical cell, where the particles are kept suspended by a stirrer.

The above process results in a very small sample of the mud fraction being analysed, *i.e.* less than 1 $cm^3$ of concentrate. In order to ensure the repeatability of the grain size distributions obtained, three different pipette samples were taken from a single mud fractions and analysed. *Figure C.1* shows that the mean grain diameters of three pipette samples vary by less than 2 μm. While two of the samples are highly repeatable, the third displays a lower percentage of coarser particles. It is concluded that mean grain diameters resulting from the Coulter LS130 are reliable to $\pm$ 2 μm, while other grain size descriptors that depend on the tails of the distribution may be more variable.

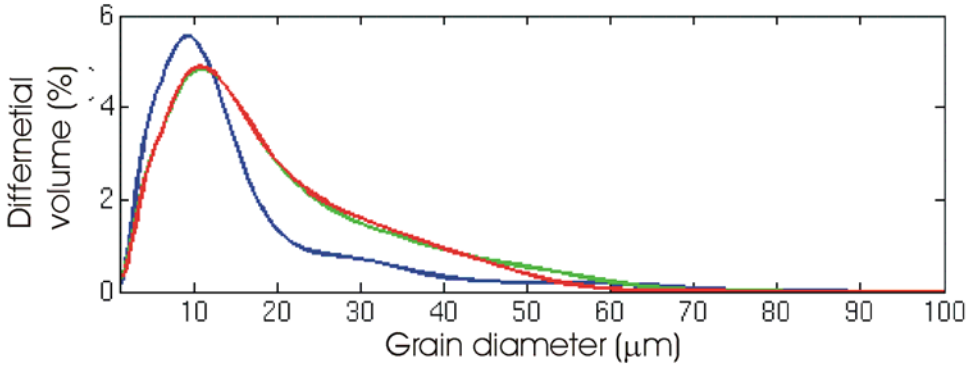


*Figure C.1. Comparison of three samples from same mud fraction in Coulter LS130, with differential volume (%) plotted against grain diameter (μm).*

The remaining mud fraction was then dried and weighed. This allowed the percentage of sand sized particles to be determined, from the dry weights of the sand and mud fractions.

It was found that the sediments examined fell into two main groups, *Section 4.4.3*. The first group were predominantly sands, *i.e.* contained less than 1.52 % muds, while the second group were predominantly muds, which contained between 3.2 % and 24 % sand sized particles. For all samples only the dominant fraction was analysed with the analysis of the lesser fraction was neglected.

The statistics applied use logarithmic graphical methods (McManus, 1989). These express the grain diameters $D$ in a logarithmic scale, named the ϕ scale, which are obtained from

$$D(\phi) = -\log_2\left(D(mm)/D_o\right) \qquad C.5,$$

where $D_o$ is the "standard" grain diameter of 1 mm and $D(mm)$ and $D(\phi)$ are in the grain diameters in units of mm and ϕ respectively. This is necessary to compact the wide range of grain sizes that may occur in typical sediment to a plotable range of values. The graphical method used constructs either a cumulative mass or volume plot, *Figure C.2,* to obtain certain percentile points from which mean grain diameter and sorting are calculated using

$$M = \frac{D_{16} + D_{50} + D_{84}}{3} \qquad C.6,$$

$$\sigma = \frac{D_{84} - D_{16}}{4} + \frac{D_{95} - D_5}{6.6} \qquad C.7,$$

where $D_x$ denotes the grain diameter in units of ϕ corresponding to the *xth* percentage point. Literature highlights that mean grain sizes represent the grain size distribution more accurately than median grain sizes (Horn *et al.*, 1968; Leeder, 1982). Additional parameters such as skewness and kurtosis are beyond the scope of this thesis.

If the undefined regions at the edges of the distribution account for greater than 1 % of the distribution, as is the case for the sediment samples analysed in this project, such graphical methods are advantageous over moment methods (McManus, 1989). The reliability of moment methods decreases sharply as the proportions of undefined material

increases. The mean grain size is the most reliable measure of the average grain size, with mode and median values becoming unreliable in the case of polymodal distributions (McManus, 1989). The sorting represents the standard deviation, or spread, of the distribution, with well-sorted sediments approximating to a single size and having low $\sigma$ values.

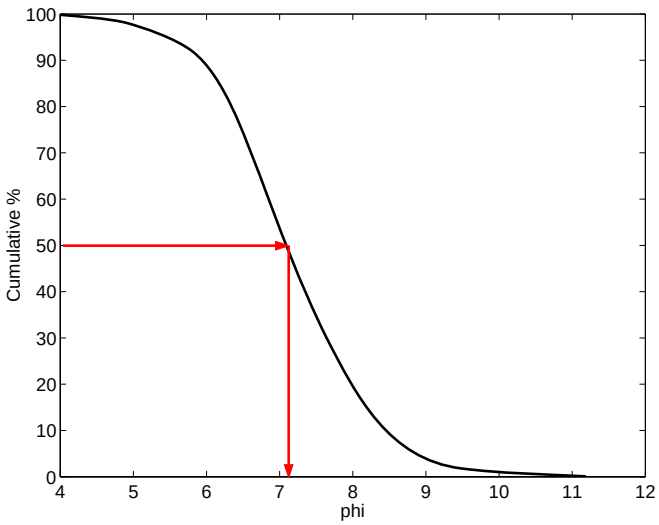


*Figure C.2. Typical cumulative percentage plot for fine-grained sediment. Arrows display $D_{50}$, i.e. the grain diameter in units of $\phi$ corresponding to the 50 % point, which is equal to 7.15$\phi$ for the distribution displayed.*

The sediment was classified according to (Friedman and Sanders, 1978), *Table C.2*, while descriptive terms applied to ranges of sorting values are displayed in *Table C.3*. Typical grain size distributions are displayed for a bimodal medium sand (*Figure C.3);* a unimodal, well sorted, fine sand (*Figure C.4*) and a unimodal, poorly sorted, medium silt (*Figure C.5*). The more detailed nature of the distribution for the medium silt is a consequence of the finer resolution of the Coulter LS130 analyser as opposed to the use a ¼ $\phi$ sieve stack.

| Mean diameter (ϕ) | Mean diameter (mm) | Sediment classification | |
|---|---|---|---|
| <-11 | >2048 | Very large | Boulders |
| -11<ϕ<-10 | 2048 - 1024 | Large | |
| -10<ϕ<-9 | 1024 –512 | Medium | |
| -9<ϕ<-8 | 512 –256 | Small | |
| -8<ϕ<-7 | 256 – 128 | Large | Cobbles |
| -7<ϕ<-6 | 128 – 64 | Small | |
| -6<ϕ<-5 | 64 – 32 | Very coarse | Pebbles |
| -5<ϕ<-4 | 32 – 16 | Coarse | |
| -4<ϕ<-3 | 16 – 8 | Medium | |
| -3<ϕ<-2 | 8 – 4 | Fine | |
| -2<ϕ<-1 | 4 – 2 | Very fine | |
| -1<ϕ<0 | 2 – 1 | Very coarse | Sand |
| 0<ϕ<1 | 1 – 0.5 | Coarse | |
| 1<ϕ<2 | 0.5 – 0.25 | Medium | |
| 2<ϕ<3 | 0.25 – 0.125 | Fine | |
| 3<ϕ<4 | 0.125 – 0.062 | Very fine | |
| 4<ϕ<5 | 0.062 – 0.031 | Very coarse | Silt |
| 5<ϕ<6 | 0.031 – 0.016 | Coarse | |
| 6<ϕ<7 | 0.016 – 0.008 | Medium | |
| 7<ϕ<8 | 0.008 – 0.004 | Fine | |
| 8<ϕ<9 | 0.004 – 0.002 | Very fine | |
| ϕ>9 | <0.002 | - | Clay |

*Table C.2. Sediment classes as defined by (Friedman and Sanders, 1978).*

| Classification | Range of sorting values |
|---|---|
| Very well sorted | < 0.35 |
| Well sorted | 0.35 – 0.50 |
| Moderately well sorted | 0.50 – 0.70 |
| Moderately sorted | 0.70 – 1.00 |
| Poorly sorted | 1.00 – 2.00 |
| Very poorly sorted | 2.00 – 4.00 |
| Extremely poorly sorted | > 4.00 |

*Table C.3. Descriptive terms applies to sorting, from (Leeder, 1982).*

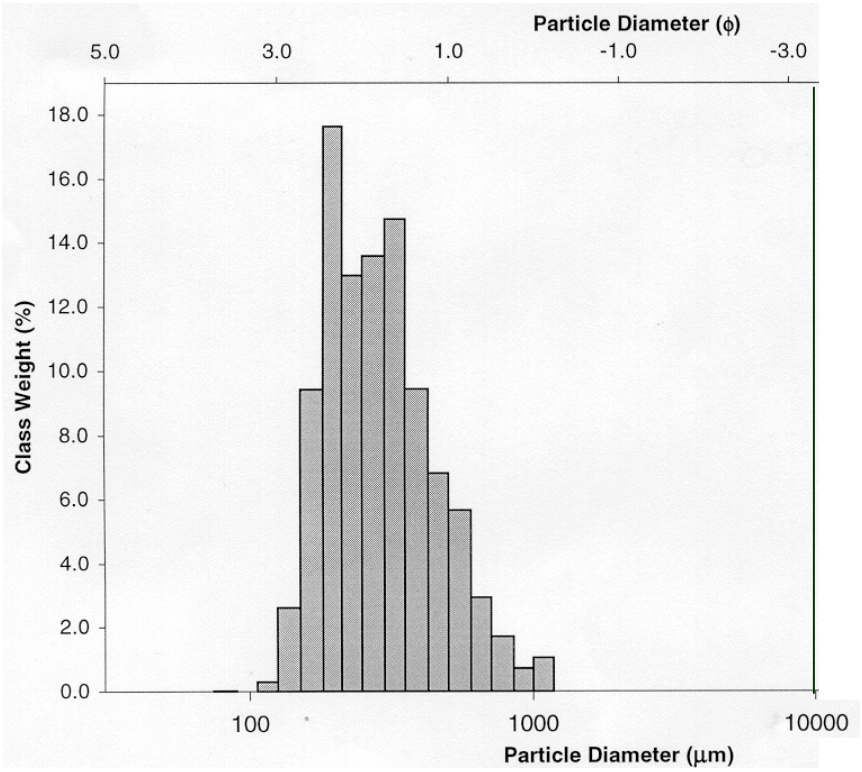


*Figure C.3. Typical grain size distribution bimodal medium sand, obtained from Studland 4.*

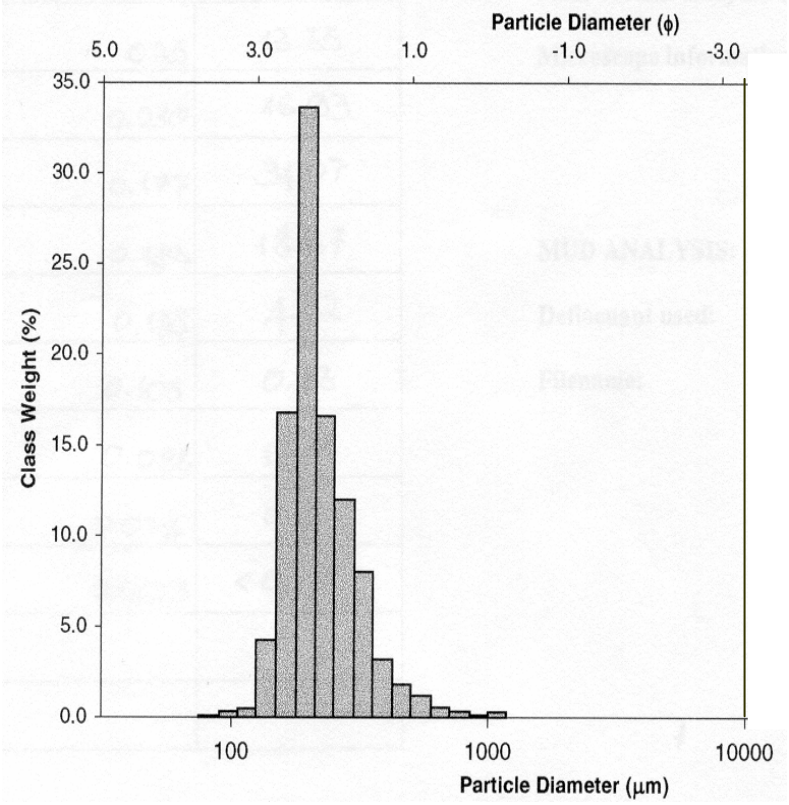


*Figure C.4. Typical grain size distribution of unimodal, well sorted fine sand, obtained from Lilliput 2.*

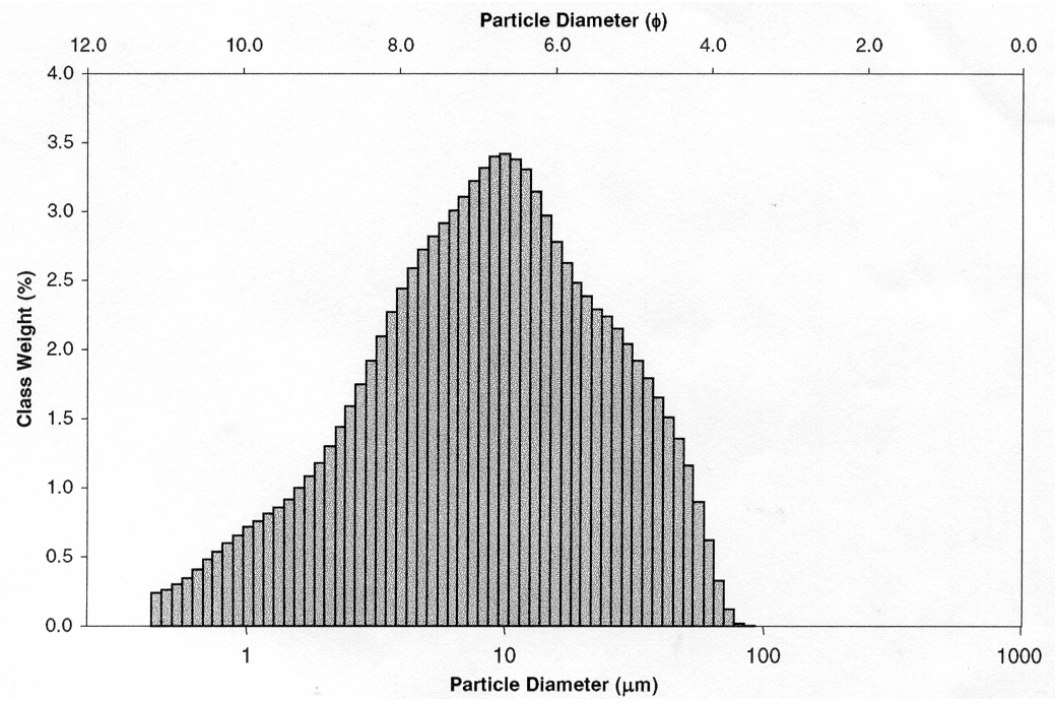


*Figure C.5. Typical grain size distribution of unimodal, poorly sorted, medium silt, from Needs Ore 3.*

## Appendix D: Data anomalies

Compressional wave properties obtained at certain locations and frequencies were considered to be corrupted and hence omitted from the analysis and discussion undertaken in *Sections 6* and *7*. Such data includes

Frequencies and locations at which an elongated received pulse, *i.e.* those which have been spread in time with respect to the *voltage output pulse* (*Figure 5.13E),* was observed. These include frequencies less than 20 kHz at Studland 4, less than 26 kHz at Studland 2, less than 20 kHz at Lilliput 1 and Needs 2. This time-spreaded pulse may incorporate additional reflected/scattered signals and so result in incorrect estimates of velocity, attenuation coefficient or quality factor.

- Frequencies less than 45 kHz at Studland 3, owing to bed scouring which reduced the depth of the probes to 0.8 m, *Appendix* 2. Hence interference between the directly transmitted wave and the wave reflected from the sediment surface may account for the fluctuations in velocity below 45 kHz, *Figure 6.1A,* and the peak in attenuation coefficient at 28 kHz, *Figure 6.1B*.

- Frequencies less than 60 kHz at Branksome 1. This is a consequence of a fault in the receiver electronics, which produced electronic noise that obscured the directly transmitted pulse. The fluctuations in velocity at frequencies less than 60 kHz, *Figure 6.2A,* and transition in attention coefficient and quality factor below 52 kHz, *Figures 6.2B* and *6.2C* respectively, is attributed to the influence of this electronic noise.

- All frequencies at Lilliput 2. This is attributed to the examination of only 3 S-R separations which produced a large scatter in velocities, Figures 6.3A, and large errors in attenuation coefficients, Figure 6.3B.

- All frequencies at Mercury 1 and 3 owing to a received signal in which the directly transmitted pulse was frequently unresolvable from additional arrivals. Such disruptions resulted in the large degree of scatter in the observed velocities, at Location 1 (1050 to 1650 $m \cdot s^{-1}$) and at Location 2 (1271 to 1452 $m \cdot s^{-1}$), and the lack of a consistent increase in attenuation coefficient with frequency, *Figure 6.5.B*. No quality factors are plotted for Location 3 owing to the low attenuation coefficients generating errors in quality factor of $\pm$ 1000. The source of the additional arrivals was attributed to pulses scattered/reflected from heterogeneities in the sediment. Such heterogeneities included larger scale rubble

and debris at both locations and gas bubbles at Location 1, the release of which were observed on probe insertion. Gas bubbles in shallow marine sediments are generally produced biogenically (Tuffin, 2001), a process which requires a source of organic matter [Claypool, 1974 #15]. Evidence of suitable organic matter, *i.e.* wood fragments and root material, were observed within the sediment examined, with rubble observed in at least the upper 50 cm of the sediment.

- Frequencies greater than 83 kHz at Needs 3 because of a poor SNR.

## Appendix E: Chi-square $\chi^2$ distribution

In order to test the validity of hypothesised frequency-dependences to the compressional wave properties measured within this project chi-square $\chi^2$ statistics were used. The $\chi^2$ value represents a weighted measure of the deviations between the measured values and hypothesised values and was computed from

$$\chi^2 = \sum_i \frac{(y_i - Y_i)^2}{\sigma_i^2} \qquad E.1,$$

where $y_i$ is the $i^{th}$ measured value, $Y_i$ is the corresponding value predicted by the weighted mean or weighted linear least-squares fit and $\sigma_i$ is corresponding error in $y_i$ (Dietrich, 1991). The $\chi^2$ value was then converted into a probability threshold, or confidence limit, using *Table E.1*. This conversion depends on the number of degrees of freedom of each fit, which equals the number of measured values less the number of parameters fitted. For example if a $\chi^2$ value of 17.000 is obtained for the application of a linear fit to 31 points (30 degrees of freedom) this indicates a probability value lying between 95 and 97.5 %, *i.e.* between 95 and 97.5 % confidence that the deviations of the observed values from the predicted fit are due to random fluctuations. The above statistics assume that the measured values are independent.

| Nos. of degrees of freedom | Prob. 80.0 % | Prob. 90.0 % | Prob. 95.0 % | Prob. 97.5 % | Prob. 99.0 % | Prob. 99.5 % |
|---|---|---|---|---|---|---|
| 10 | 6.179 | 4.865 | 3.940 | 3.247 | 2.558 | 2.156 |
| 11 | 6.989 | 5.578 | 4.575 | 3.816 | 3.053 | 2.603 |
| 12 | 7.807 | 6.304 | 5.226 | 4.404 | 3.571 | 3.074 |
| 13 | 8.634 | 7.042 | 5.892 | 5.009 | 4.107 | 3.565 |
| 14 | 9.467 | 7.790 | 6.571 | 5.629 | 4.660 | 4.075 |
| 15 | 10.307 | 8.547 | 7.261 | 6.262 | 5.229 | 4.601 |
| 16 | 11.152 | 9.312 | 7.962 | 6.908 | 5.812 | 5.142 |
| 17 | 12.002 | 10.085 | 8.672 | 7.564 | 6.408 | 5.697 |
| 18 | 12.857 | 10.865 | 9.390 | 8.231 | 7.015 | 6.265 |
| 19 | 13.716 | 11.651 | 10.117 | 8.907 | 7.663 | 6.844 |
| 20 | 14.578 | 12.443 | 10.851 | 9.951 | 8.260 | 7.434 |
| 25 | 18.940 | 16.473 | 14.611 | 13.102 | 11.524 | 10.520 |
| 30 | 23.364 | 20.599 | 18.493 | 16.791 | 14.953 | 13.787 |
| 35 | 27.836 | 24.797 | 22.465 | 20.569 | 18.509 | 17.192 |
| 40 | 32.345 | 29.051 | 26.509 | 24.433 | 22.164 | 20.707 |
| 45 | 36.884 | 33.350 | 30.612 | 28.361 | 25.901 | 24.311 |

*Table E.1. Table used to convert $\chi^2$ values and nos. of degrees of freedom to a percentage confidence limit, from (Dietrich, 1991).*